FREE VIBRATION ANALYSIS OF ORTHOTROPIC RECTANGULAR PLATES USING THE RITZ NUMERICAL METHOD

UDC:534-16:519.6
Original scientific paper https://doi.org/10.46793/adeletters.2023.2.4.2

K. Dileep Kumar[1*]

[1]University College of Engineering Kakinada, Jawaharlal Nehru Technological University, Kakinada, India

Abstract:
The main objective of this paper is to contribute to a better understanding of the dynamic response of FRP rectangular plates through modal analysis. The Ritz's approximation method originated from the principle of minimum potential energy and was chosen to formulate the Eigenvalue problem. The natural frequencies and mode shapes are determined for the first 36 free vibration modes by assuming the double Fourier series functions for the transverse displacement. The most common Beam functions are used as a functional basis. Results are shown for the specific plate problem of Angle ply rectangular plate clamped at one edge, supported at two adjacent edges, and accessible at another edge (CSSF). It is observed that maximum natural frequencies are obtained under the clamped boundary of the plate on all edges of (CCCC) for the rectangular laminates.

ARTICLE HISTORY
Received: 11 August 2023
Revised: 26 October 2023
Accepted: 29 November 2023
Published: 31 December 2023

KEYWORDS
Vibrations, laminated plate, boundary conditions, Ritz method, beam functions, mode shapes

1. INTRODUCTION

There are two main methods to address engineering problems in general, namely, analytical and numerical methods. Analytical methods give closed-form solutions to the problems. However, they are only sometimes easily attainable for plates with mixed boundary conditions, discontinuities at their edge support, and plates with irregular boundaries. Though analytical methods are preferable, they become cumbersome sometimes due to the difficulty of satisfying the governing differential equations with anticipated boundary conditions. So, the numerical techniques provide quick approximate solutions close to exact solutions without affecting the accuracy of the solution.

Much work on the damping analysis utilizing Ritz's method has been cited in the literature. The limitation of damping characteristics has been discussed in papers [1-3]. Damping characters are predicted experimentally and analytically for the interleaved viscoelastic orthotropic plates in [4], respectively. Fasana et al. [5] used the Rayleigh-Ritz method to predict the dynamic behavior of beams. Narita [6] used Ritz's method to calculate the frequencies of anisotropic rectangular plates for different boundary conditions. Bahrami et al. [7] have attempted to predict the model properties of free-free FRP plates using the Finite Element Method. Ritz's method is a well-known approximate method used for over a century in classical mechanics and has been successfully implemented in the vibration analysis of beams and plates [8, 9]. This method with geometrically admissible functions always gives upper-bound solutions.

Liu and Banerjee [10] introduce a novel spectral-dynamic stiffness method for free vibration analysis of plates with arbitrary boundary conditions. The research enhances the analytical methods available for studying plate vibrations. He et al. [11] investigate in-plane vibrations of rectangular plates with periodic homogeneity. He, Chen, and Qiao provide insights into natural frequencies and their adjustment, contributing to understanding composite plate dynamics. Shi et al. [12] present a unified method for free vibration analysis of circular, annular, and sector plates with arbitrary boundary

*CONTACT: K. Dileep Kumar, e-mail: davidkumar999@jntucek.ac.in

conditions. This study expands the analytical methods for diverse plate geometries. Najarzadeh et al. [13] explore the free vibration and buckling analysis of thin plates subjected to high gradient stresses, employing a combination of finite strip and boundary element methods. This research provides insights into plate behavior under extreme loading conditions.

Mahapatra and Panigrahi [14] analyze the dynamic response and vibration power flow of rectangular isotropic plates using the Fourier series approximation and a mobility approach. This research contributes to understanding isotropic plates' energy transfer and response characteristics. Li et al. [15] investigate the vibration analysis of functionally graded porous cylindrical shells; Li et al. employ a semi-analytical method. This study extends the understanding of composite shell vibrations, specifically considering porosity and material gradients. Li et al. [16] present new analytic free vibration solutions for orthotropic rectangular plates using a novel symplectic approach. The research introduces innovative methods for analyzing the vibrational behavior of orthotropic plates.

Zhang et al. [17] contribute new exact series solutions for the transverse vibration of rotationally-restrained orthotropic plates. This research enhances the analytical methods available for understanding the transverse vibration characteristics of orthotropic plates, particularly when subject to rotational restraints. Chen et al. [18] propose an iso-geometric finite element method for the in-plane vibration analysis of orthotropic quadrilateral plates with general boundary restraints. The study presents an innovative numerical approach, providing a valuable tool for analyzing the vibrational behavior of orthotropic plates with complex boundary conditions.

Amidst the existing research endeavors, a predominant focus has been directed toward exploring transverse vibrations in plates, leaving the domain of in-plane vibration research to be more represented. In papers [19-21], authors introduce the analytical symplectic superposition method to derive free vibration solutions for rectangular plates. Additionally, authors in papers [17] employ a finite integral transform solution to discern the vibration behavior of rectangular orthotropic thin plates under diverse boundary conditions. In papers [22, 23], authors extend the integral transform method to scrutinize the buckling behavior of rectangular plates. While numerous other commendable achievements exist, a detailed discussion on each is beyond the scope of this overview.

In this paper, an attempt is made to extend Ritz's methodology for the modal analysis of laminated plates. The analysis in the study is carried out for an eight-layered Glass/Epoxy rectangular laminated plate with length *a*=0.38 m, width *b*=0.3 m and thickness *h*=0.0024 m. Properties of Glass/Epoxy material are given in Table 1. Three different plate configurations, namely, unidirectional - [0º 0 º 0 º 0 º]s, cross-ply - [0 º 90 º 0 º 90º]s and angle ply - [45º 30º -30º 90º]s symmetric laminates under different boundary conditions are considered for the study.

2. THE RITZ METHOD

For a laminated plate, the maximum Potential Energy in terms of the plate transverse displacement '*w*' and bending stiffness is:

$$U = \frac{1}{2}\iint \left\{ D_{11}\left(\frac{\partial^2 w}{\partial x^2}\right)^2 + 2D_{12}\frac{\partial^2 w}{\partial x^2}\frac{\partial^2 w}{\partial y^2} + D_{22}\left(\frac{\partial^2 w}{\partial y^2}\right)^2 + 4D_{66}\left(\frac{\partial^2 w}{\partial x \partial y}\right)^2 \right\} dxdy \quad (1)$$

and the maximum Kinematic Energy is:

$$T = \frac{1}{2}\rho h\omega^2 \iint w^2\, dxdy \quad (2)$$

In the lamination theory, the bending stiffness matrix which relates the stress couples to the plate curvatures is given by:

$$[D_{ij}] = \frac{1}{3}\sum_{k=1}^{N} \overline{[Q_{ij}]}^{(k)} (Z_k^3 - Z_{k-1}^3)$$

where:

$$\overline{[Q_{ij}]}^{(k)} = \left[T_m^{(k)}\right]^{-1}\left[TQ^{(k)}\right][R]\left[T_m^{(k)}\right][R]^{-1} \quad (3)$$

The matrix $[\overline{Q_{ij}}]$ is the reduced stiffness matrix, which is determined using the transformation matrix $[T_m]$:

$$\left[T_m^{(k)}\right] = \begin{bmatrix} cos^2\,\theta_k & sin^2\,\theta_k & 2\,cos\,\theta_k\,sin\,\theta_k \\ sin^2\,\theta_k & cos^2\,\theta_k & -2\,cos\,\theta_k\,sin\,\theta_k \\ -\,cos\,\theta_k\,sin\,\theta_k & cos\,\theta\,sin\,\theta_k & cos^2\,\theta_k - sin^2\,\theta_k \end{bmatrix} \quad (4)$$

[R] is known as the Reuter matrix and is given by:

$$[R] = \begin{bmatrix} 1 & 0 & 0 \\ 0 & 1 & 0 \\ 0 & 0 & 2 \end{bmatrix} \quad (5)$$

and the stiffness coefficients are given by:

$$\left[Q^{(k)}\right] = \begin{bmatrix} \frac{E_L^{(k)}}{\left(1-\vartheta_{LT}^{(k)}\vartheta_{TL}^{(k)}\right)} & \frac{E_T^{(k)}\vartheta_{LT}^{(k)}}{\left(1-\vartheta_{LT}^{(k)}\vartheta_{TL}^{(k)}\right)} & 0 \\ \frac{E_L^{(k)}\vartheta_{TL}^{(k)}}{\left(1-\vartheta_{LT}^{(k)}\vartheta_{TL}^{(k)}\right)} & \frac{E_T^{(k)}}{\left(1-\vartheta_{LT}^{(k)}\vartheta_{TL}^{(k)}\right)} & 0 \\ 0 & 0 & G_{LT}^{(k)} \end{bmatrix} \quad (6)$$

It is a known fact that the system's total energy is constant at any time, which means:

$$U = T \text{ or } U - T = Constant \tag{7}$$

The series approximation considered in Ritz's method is:

$$w(x,y) = \sum_{m=1}^{P} \sum_{n=1}^{Q} A_{mn} \cdot X_m(x) \cdot Y_n(y) \tag{8}$$

where X_m and Y_n are the admissible functions that form the functional basis and A_{mn} represents the amplitude coefficients to be determined. *P* and *Q* are the limits of series expression whose product gives the number of modes that can be studied, and as they increase in value, the accuracy of the results would increase. In general, they can take values like *P*=3 and *Q*=3 gives 9 modes of frequencies; *P*=3 and *Q*=6 results in 18 different modes. In this investigation, *P* and *Q* are taken to be 6 and this gives a total of 36 vibrational frequency modes.

Applying the law of conservation of energy is shown as follows:

$$\frac{\partial U}{\partial A_{ik}} - \frac{\omega^2 \rho h}{2} \frac{\partial}{\partial A_{ik}} \iint w^2 dxdy = 0 \tag{9}$$

where A_{ik} is any one of the coefficients A_{mn}.

The solution of the equation (9), a system of linear homogeneous equations with A_{mn} as unknowns. The natural frequencies (ω_1, ω_2 …) are determined by taking the condition that the determinant of the system must vanish. Table 1 shows the properties of the material that is used.

Table 1. Properties of Glass/Epoxy material

Control factors	Units	Level I
(A) Longitudinal Modulus	E_L (GPa)	29.9
(B)Transverse Modulus	E_T (GPa)	5.85
(C) Shear Modulus	G_{LT} (GPa)	2.4
(D) Density	ρ (kg/m^3)	1560
(F) Poisons ratio	ϑ_{LT}	0.24

3. FUNCTIONAL BASIS

Different types of beams are distinguished by their end conditions. A beam can have infinite normal modes shown by its transverse oscillations. The method of determining the set of characteristic functions that define these normal modes for any type of beam is available in standard references such as [7, 8]. Also, this issue is discussed in the standard textbook by Jean Marie Berthelot. The characteristic functions for the six types of beams used are as follows:

3.1 Beam Functions for C-C, C-S, C-F, S-S and S-F Combinations

For clamped edges at *x=0* and *x=a*:

$$X_m(x) = cosh\,\lambda_m \frac{x}{a} - cos\,\lambda_m \frac{x}{a} - \gamma_m \left(sinh\,\lambda_m \frac{x}{a} - sin\,\lambda_m \frac{x}{a} \right) \tag{10}$$

In the similar way, equation for $Y_n(y)$ is obtained.

3.2 Free-Free Beam Functions

For free edges at *x=0* and *x=a*:

$$X_1(x) = 1 \tag{11}$$

$$X_2(x) = \sqrt{3}\left(1 - 2\frac{x}{a}\right) \tag{12}$$

$$X_m(x) = cosh\,\lambda_m \frac{x}{a} + cos\,\lambda_m \frac{x}{a} - \gamma_m \left(sinh\,\lambda_m \frac{x}{a} + sin\,\lambda_m \frac{x}{a} \right) \tag{13}$$

Lambda and Gamma values for various boundary conditions were evaluated using MATLAB code and presented in Table 2.

Table 2. Values of and for 3-different Boundary Conditions

Type of Beam	m (or) n	Lambda (λ)	Gamma (γ)
(A) Clamped-Clamped	1	$4.7302e+00$	$9.8250e-01$
	2	$7.8534e+00$	$1.0007e+00$
	3	$1.0995e+01$	$9.9996e-01$
	4	$1.4132e+01$	$1.0000e+00$
	5	$1.7275e+01$	$9.9999e-01$
	6	$2.0427e+01$	$1.0000e+00$
	7	$2.3563e+01$	$9.9999e-01$
	8	$2.6701e+01$	$1.0000e+00$
	9	$2.9058e+01$	$1.0000e+00$
	10	$3.2209e+01$	$1.0000e+00$
(B) Clamped-Simply Supported	1	$3.9331e+00$	$7.3409e-01$
	2	$7.0685e+00$	$1.0184e+00$
	3	$1.0210e+01$	$9.9922e-01$
	4	$1.3345e+01$	$1.0000e+00$
	5	$1.6487e+01$	$9.9999e-01$
	6	$1.9628e+01$	$1.0000e+00$
	7	$2.2770e+01$	$9.9999e-01$
	8	$2.5918e+01$	$1.0000e+00$
	9	$2.9059e+01$	$1.0000e+00$
	10	$3.2201e+01$	$1.0000e+00$
(C) Clamped-Free	1	$1.8752e+00$	$7.3409e-01$
	2	$4.6939e+00$	$1.0184e+00$
	3	$7.8555e+00$	$9.9922e-01$
	4	$1.0994e+01$	$1.0000e+00$
	5	$1.41379e+01$	$9.9999e-01$
	6	$1.7278e+01$	$1.0000e+00$
	7	$2.04211e+01$	$9.9999e-01$
	8	$2.3561e+01$	$1.0000e+00$
	9	$2.9059e+01$	$1.0000e+00$
	10	$3.2201e+01$	$1.0000e+00$

4. DETERMINATION OF A_{mn} AND NATURAL FREQUENCIES

By using Equations (1) to (8), the set of Equations (9) can be reduced to a very simplified form as

$$\sum_{m=1}^{P}\sum_{n=1}^{Q}[C_{mn}^{(ik)} - \lambda C_{mink}^{0000}]\,A_{mn} = 0 \qquad (14)$$

$$\text{where } \lambda = \omega^2 \rho h a^3 b \text{ and } \omega = 2\pi f \qquad (15)$$

where is the angular frequency in rad/sec and *f* is the frequency in Hz.

$$C_{mink}^{0000} = 1 \text{ for } mn = ik$$

$$C_{mink}^{0000} = 0 \text{ for } mn \neq ik \text{ and}$$

$$C_{mn}^{(ik)} = \left\{\frac{b}{a}D_{11}C_{mink}^{2200} + \frac{a^3}{b^3}D_{22}C_{mink}^{0022} + \frac{a}{b}D_{12}[C_{mink}^{2002} + C_{mink}^{0220}] + 4D_{66}\frac{a}{b}C_{mink}^{1111}\right\} \qquad (16)$$

Equation (14) gives as many equations as *P·Q* with each *'ik';* the characteristic values λ from the condition that the determinant of this system of equations must vanish. When there are more than three equations in the system, it is not advisable to go for mathematical expansion of the determinant and solve for the roots of the polynomial in λ. In such cases, it is suggested to solve for λ by iterative procedures. One of the advantages of using beam functions for X_m and is Y_n that the diagonal terms in the determinant are significant compared to other terms. So, the characteristic values and modes can be found by following the simple iteration procedure Ritz used [6].

Using the Equation (16), $C_{mn}^{(ik)}$ values are calculated. For each combination of 'ik' with a total range of *P·Q*, *P·Q* number of $C_{mn}^{(ik)}$ coefficient values are obtained. So the total number of $C_{mn}^{(ik)}$ would be *P·Q* by *P·Q*. The next step is to form the system of equations from the Equation (14).

Total *P·Q* equations with each combination of *'ik'* were obtained, as shown:

$$(C_{11}^{11} - \lambda)A_{11} + C_{12}^{11}A_{12} + C_{13}^{11}A_{13} + \cdots + C_{21}^{11}A_{21} + C_{22}^{11}A_{22} + \cdots = 0$$

$$C_{11}^{12}A_{11} + (C_{12}^{12} - \lambda)A_{12} + C_{13}^{12}A_{13} + \cdots + C_{21}^{12}A_{21} + C_{22}^{12}A_{22} + \cdots = 0 \qquad (17)$$

$$C_{11}^{13}A_{11} + C_{12}^{13}A_{12} + (C_{13}^{13} - \lambda)A_{13} + \cdots + C_{21}^{13}A_{21} + C_{22}^{13}A_{22} + \ldots = 0.$$

First, the diagonal terms of the obtained values of the coefficient $C_{mn}^{(ik)}$ are examined, which means that it is necessary to move from the lowest frequency to higher modes. Then the predominant amplitude coefficient A_{mn} corresponding to the most negligible value from the $C_{mn}^{(ik)}$ coefficients is identified and its value is taken as unity for each mode. If it is taken that A_{11}=1, the above system of equations (17) is rearranged as follows:

$$\lambda = C_{11}^{11} + C_{12}^{11}A_{12} + C_{13}^{11}A_{13} + \ldots + C_{21}^{11}A_{21} + C_{22}^{11}A_{22} + \cdots \qquad (18a)$$

$$A_{12} = -(C_{11}^{12} + C_{13}^{12}A_{13} + \ldots\ldots\ldots + C_{21}^{12}A_{21} + C_{22}^{12}A_{22} + \ldots)/(C_{12}^{12} - \lambda) \qquad (18b)$$

$$A_{13} = -(C_{11}^{13} + C_{12}^{13}A_{12} + \ldots + C_{21}^{13}A_{21} + C_{22}^{13}A_{22} + \ldots)/(C_{13}^{13} - \lambda) \qquad (18c)$$

$$A_{21} = -(C_{11}^{21} + C_{12}^{21}A_{12} + C_{13}^{21}A_{13} + \ldots + C_{22}^{21}A_{22} + \ldots)/(C_{21}^{21} - \lambda) \qquad (18d)$$

$$A_{22} = -(C_{11}^{22} + C_{12}^{22}A_{12} + C_{13}^{22}A_{13} + \ldots + C_{21}^{22}A_{21} + \ldots)/(C_{22}^{22} - \lambda) \qquad (18e)$$

For the first trace in this iterative procedure, the initial values for A_{12}, A_{13},… A_{21}, A_{22} are taken as zero. The first trail value is calculated from Equation (18a) and then A_{12} is calculated from Equation (18b). Using this improved value of A_{12} and the first trail values for other A_{mn}, A_{13} is calculated from Equation (18c). This procedure is continued for all the remaining equations. After obtaining all the improved values for A_{mn}, they are substituted back into Equation (18a) to get a second trail value for λ. Again, the same procedure is repeated to calculate A_{12}, A_{13},… A_{21}, A_{22}. The procedure is repeated till the values of λ and A_{mn} are close enough in the successive iterations to give the required accuracy.

The same procedure is applied for the higher frequencies. The next predominant amplitude coefficient is identified and its value is taken as unity. After calculating the λ values, natural frequencies (ω) can be calculated from equation (15). Knowing the relative values of A_{mn} and the beam functions X_m and Y_n, the shape of each vibrational mode can be obtained from Equation (8). Lambda and Gamma values for various boundary conditions were evaluated using MATLAB code and presented in the Table 3.

Table 3. Values of and for other 3-different Boundary Conditions

Type of Beam	m (or) n	Lambda (λ)	Gamma (γ)
(A) Simply Supported-Simply Supported	1	$3.9270e+00$	$1.0007e+00$
	2	$7.0685e+00$	$1.0000e+00$
	3	$1.0210e+01$	$1.0000e+00$
	4	$1.3351e+01$	$9.9999e-01$
	5	$1.6493e+01$	$1.0000e+00$
	6	$1.9634e+01$	$9.9999e-01$
	7	$2.2776e+01$	$1.0000e+00$
	8	$2.5918e+01$	$1.0000e+00$
	9	$2.9059e+01$	$1.0000e+00$
	10	$3.2201e+01$	$1.0000e+00$
(B) Simply Supported-Free	1	$1.8752e+00$	$7.3409e-01$
	2	$4.6939e+00$	$1.0184e+00$
	3	$7.8555e+00$	$9.9922e-01$
	4	$1.0994e+01$	$1.0000e+00$
	5	$1.4137e+01$	$9.9999e-01$
	6	$1.7278e+01$	$1.0000e+00$
	7	$2.0421e+01$	$9.9999e-01$
	8	$2.3561e+01$	$1.0000e+00$
	9	$2.9059e+01$	$1.0000e+00$
	10	$3.2201e+01$	$1.0000e+00$
(C) Free-Free	1	0	0
	2	0	0
	3	$4.7300e+00$	$9.8252e-01$
	4	$7.8532e+00$	$1.0007e+00$
	5	$1.0995e+01$	$9.9996e-01$
	6	$1.4137e+01$	$1.0000e+00$
	7	$1.7278e+01$	$9.9999e-01$
	8	$2.0420e+01$	$1.0000e+00$
	9	$2.9059e+01$	$1.0000e+00$
	10	$3.2201e+01$	$1.0000e+00$

5. RESULTS AND DISCUSSION

5.1 Application of the Ritz Method

An Angle ply plate- [45° 30° -30° 90°]s which is clamped at the end x=0, simply supported at x=1 and y=0 and free at the end y=1. It is Clamped-Simply Supported in X-direction and Simply Supported-Free in Y-direction. Equation (10) is to be taken for X_m and Y_n. The calculations for this problem is carried out for P=6 and Q=6 by taking m and n equal to 1, 2, 3, 4, 5, 6 which gives a 36-term series based solution. The fibre orientation is θ=0°. Using the properties of Glass/Epoxy material, [Q] matrix can be obtained. From [Q] matrix and transformation matrix, [$\overline{Q}$] matrix is calculated, which in turn is used in finding the [D] matrix from Equation (3). The amplitude coefficient corresponding to each pair of lambda and gamma for various combinations of boundary conditions is shown in Table 4.

Equation (14) gives a system of 36 equations with A_{mn} as unknowns. The predominant amplitude coefficients are selected by examining the diagonal terms of $C_{mn}^{(ik)}$ and the iterative procedure is followed to obtain natural frequencies and mode shapes of first 36 modes. The Amplitude Coefficients of the first five modes and their frequency values are shown in Table 4 and Table 5. Mode shapes are the pattern of displacement used to identify the severely loaded locations during oscillation for the first five modes, shown in Figs. 1-5, respectively. The free boundary displaces more and produces severe conditions for failure owing to its high flexibility. The uniqueness of mode shape in vibration performance was shown above clearly shown in Figs.1-5.

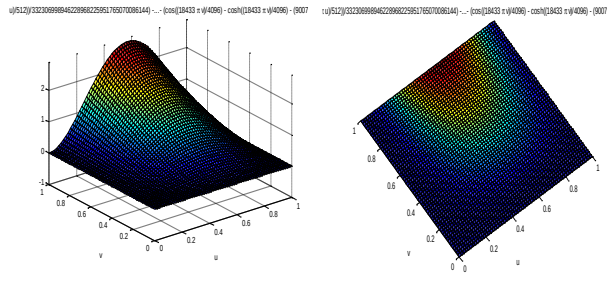

Fig. 1. Mode 1 for CSSF: 3D-Mode and Top View of Mode

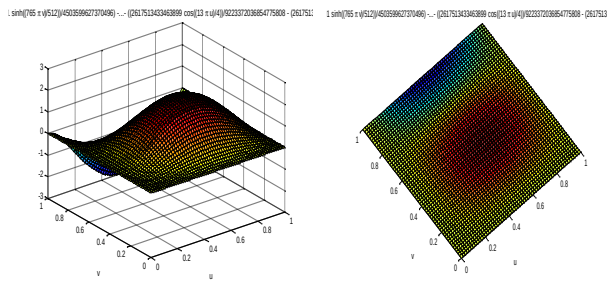

Fig. 2. Mode 2 for CSSF: 3D-Mode and Top View of Mode

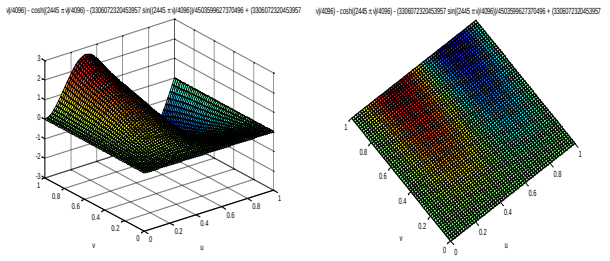

Fig. 3. Mode 3 for CSSF: 3D-Mode and Top View of Mode

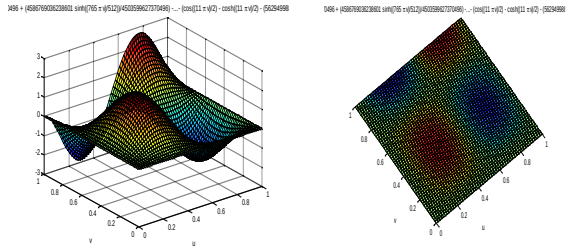

Fig. 4. Mode 4 for CSSF: 3D-Mode and Top View of Mode

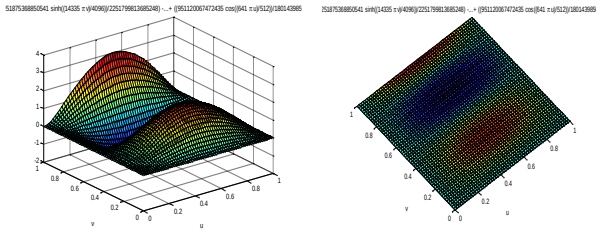

Fig. 5. Mode 5 for CSSF: 3D-Mode and Top View of Mode

Sometimes, mode shape repetition may be observed for two consecutive modes as we keep moving from Mode 1 to Mode 36. For example, let us assume that mode shapes for A_{mn} and A_{ik} are in match. To avoid such cases, once it is taken as $A_{mn}=1$ and $A_{ik}=1$. Both are taken as unity where is the dominant coefficient and when A_{ik} is A_{mn} the dominant amplitude, it is taken as A_{ik}=1 and A_{mn}=-1. The first case would result in the same mode shape which seemed to be a match, and the latter case would change the orientation of the mode shape. The frequency values remain unchanged.

Table 4. Amplitude Coefficients (A_{mn}) for Angle ply glass/epoxy laminate under CSSF

Mode 1	Mode 2	Mode 3	Mode 4	Mode 5
A_{11} = 1.00	A_{11} = -9.70e-2	A_{11} = -1.83e-2	A_{11} = 1.50e-2	A_{11} = -5.87e-3
A_{12} = 9.6e-2	A_{12} = 1.00	A_{12} = 2.28e-2	A_{12} = -8.61e-2	A_{12} = -9.04e-2
A_{13} = 1.5e-2	A_{13} = 8.91e-2	A_{13} = -1.37e-3	A_{13} = -4.25e-2	A_{13} = 1.00
A_{14} = -1.2e-3	A_{14} = -2.41e-3	A_{14} = -1.15e-4	A_{14} = -2.05e-3	A_{14} = 5.27e-2
A_{15} = 3.5e-3	A_{15} = 6.40e-3	A_{15} = -9.28e-4	A_{15} = -2.29e-3	A_{15} = -3.92e-3
A_{16} = -1.3e-3	A_{16} = 3.14e-4	A_{16} = 3.64e-4	A_{16} = -6.75e-4	A_{16} = 6.54e-3
A_{21} = 1.6e-2	A_{21} = -3.72e-2	A_{21} = 1.00	A_{21} = -1.58e-1	A_{21} = -2.73e-3
A_{22} = -2.8e-3	A_{22} = 8.32e-2	A_{22} = 1.53e-1	A_{22} = 1.00	A_{22} = 1.02e-2
A_{23} = -1.9e-3	A_{23} = 1.74e-3	A_{23} = 3.67e-2	A_{23} = 1.93e-1	A_{23} = 1.26e-1
A_{24} = -6.1e-6	A_{24} = -4.28e-4	A_{24} = -8.83e-4	A_{24} = 6.10e-3	A_{24} = 4.18e-3
A_{25} = -8.0e-4	A_{25} = -4.72e-4	A_{25} = 1.05e-2	A_{25} = 1.74e-2	A_{25} = 4.16e-5
A_{26} = 2.8e-4	A_{26} = -1.86e-5	A_{26} = -3.57e-3	A_{26} = 3.78e-3	A_{26} = 4.27e-4
A_{31} = 4.1e-3	A_{31} = -5.26e-3	A_{31} = 8.63e-3	A_{31} = -1.52e-2	A_{31} = -1.19e-2
A_{32} = -1.3e-3	A_{32} = 2.64e-2	A_{32} = 4.06e-4	A_{32} = 6.01e-2	A_{32} = -1.09e-2
A_{33} = -9.4e-4	A_{33} = -9.75e-4	A_{33} = -1.02e-3	A_{33} = 6.87e-3	A_{33} = 4.23e-2
A_{34} = -1.8e-5	A_{34} = -2.83e-4	A_{34} = -2.00e-4	A_{34} = -4.23e-4	A_{34} = 1.02e-4
A_{35} = -5.5e-4	A_{35} = -5.36e-4	A_{35} = -8.07e-4	A_{35} = -2.04e-5	A_{35} = -4.76e-4
A_{36} = 2.1e-4	A_{36} = -1.49e-4	A_{36} = 2.55e-4	A_{36} = -1.46e-4	A_{36} = -2.30e-4
A_{41} = 9.9e-4	A_{41} = -1.85e-3	A_{41} = 2.60e-3	A_{41} = -4.31e-3	A_{41} = -7.58e-4
A_{42} = -5.9e-4	A_{42} = 9.80e-3	A_{42} = -1.63e-5	A_{42} = 2.11e-2	A_{42} = -3.91e-3
A_{43} = -4.4e-4	A_{43} = -1.06e-3	A_{43} = -5.82e-4	A_{43} = 1.40e-3	A_{43} = 1.85e-2
A_{44} = -6.0e-6	A_{44} = -1.52e-4	A_{44} = -1.19e-4	A_{44} = -3.78e-4	A_{44} = -5.90e-4
A_{45} = -3.4e-4	A_{45} = -4.57e-4	A_{45} = -5.76e-4	A_{45} = -4.40e-4	A_{45} = -1.25e-4
A_{46} = 1.4e-4	A_{46} = -1.25e-4	A_{46} = 2.02e-4	A_{46} = -2.50e-4	A_{46} = -3.87e-4
A_{51} = 5.4e-4	A_{51} = -8.23e-4	A_{51} = 9.61e-4	A_{51} = -1.82e-3	A_{51} = -2.74e-4
A_{52} = -2.5e-4	A_{52} = 4.55e-3	A_{52} = -3.82e-5	A_{52} = 9.18e-3	A_{52} = -2.01e-3
A_{53} = -2.2e-4	A_{53} = -7.14e-4	A_{53} = -3.17e-4	A_{53} = 2.55e-4	A_{53} = 9.39e-3
A_{54} = 1.2e-6	A_{54} = -7.37e-5	A_{54} = -6.39e-5	A_{54} = -2.41e-4	A_{54} = -5.90e-4
A_{55} = -2.1e-4	A_{55} = -3.33e-4	A_{55} = -3.78e-4	A_{55} = -4.11e-4	A_{55} = -5.22e-5
A_{56} = 1.0e-4	A_{56} = -8.81e-5	A_{56} = 1.46e-4	A_{56} = -2.06e-4	A_{56} = -3.51e-4
A_{61} = 1.52e-4	A_{61} = -3.88e-4	A_{61} = 4.62e-4	A_{61} = -8.93e-4	A_{61} = -1.22e-4
A_{62} = -1.36e-4	A_{62} = 2.14e-3	A_{62} = -2.33e-5	A_{62} = 4.59e-3	A_{62} = -1.09e-3
A_{63} = -1.17e-4	A_{63} = -4.64e-4	A_{63} = -1.77e-4	A_{63} = -1.34e-6	A_{63} = 4.92e-3
A_{64} = 4.40e-6	A_{64} = -3.11e-5	A_{64} = -3.37e-5	A_{64} = -1.44e-4	A_{64} = -4.75e-4
A_{65} = -1.32e-4	A_{65} = -2.31e-4	A_{65} = -2.48e-4	A_{65} = -3.14e-4	A_{65} = -1.56e-5
A_{66} = 6.96e-5	A_{66} = -5.79e-5	A_{66} = 1.04e-4	A_{66} = -1.51e-4	A_{66} = -2.84e-4

Table 5. Angular and Natural frequencies of Angle ply glass/epoxy laminate under CSSF

The examined variable	Mode 1	Mode 2	Mode 3	Mode 4	Mode 5
Angular Frequency (rad/sec)	2.9e+02	7.3e+02	8.1e+02	1.3e+03	1.5e+03
Frequency (Hz)	4.7e+01	1.1e+01	1.2e+02	2.1e+02	2.4e+02

6. CONCLUSIONS

Thus, using an iterative procedure, the Ritz methodology has been successfully developed and implemented for laminated plates. The method can conveniently handle 36 possible combinations of boundary conditions for rectangular plates. The present numerical results are validated with the experimental results published in research [1].

Under a specific boundary condition for unidirectional laminates, the frequencies increased as the fibre orientation increased for θ = 0°, 30° and 60°. As the ϑ increased, the stiffness values improved, resulting in increased $C_{mn}^{(ik)}$ coefficients and better characteristic values λ. Among the three plate configurations considered, most boundary conditions showed better results for angle-ply laminate. This is also due to the effect of ϑ in each layer resulting in better $C_{mn}^{(ik)}$ coefficients. CCCC boundary condition showed the maximum natural frequencies among all 36 boundary conditions. As per its characteristics, CC edge condition has the maximum λ_m and γ_n values resulting in higher Beam functions. This finally provided maximum natural frequencies from the better $C_{mn}^{(ik)}$ coefficients and characteristic values λ.

It is observed that natural frequencies are sensitive to fiber orientation, laminate sequence, and boundary conditions, whereas mode shapes are strongly influenced by the boundary conditions alone.

REFERENCES

[1] J.-M. Berthelot, Damping analysis of laminated beams and plates using the Ritz method. *Composite Structures*, 74(2), 2006: 186-201. https://doi.org/10.1016/j.compstruct.2005.04.031

[2] J.-M. Berthelot, Y. Sefrani, Damping analysis of orthotropic composites with interleaved viscoelastic layers: experimental investigation and discussion. *Journal of Composite Materials*, 40(21), 2006: 1911-1932. https://doi.org/10.1177/0021998306061303

[3] J.-M. Berthelot, Damping analysis of orthotropic composites with interleaved viscoelastic layers: modelling. *Journal of Composite Materials*, 40(21), 2006: 1889-1909. https://doi.org/10.1177/0021998306061302

[4] J.-M. Berthelot, Sefrani, Y., Damping analysis of unidirectional glass and Kevlar fiber composite. *Composite Science and Technology*, 64(9), 2004: 1261-1278. https://doi.org/10.1016/j.compscitech.2003.10.003

[5] A. Fasana, S. Marchesiello, Rayleigh-Ritz Analysis of Sandwich beams. *Journal of Sound Vibrations*, 241(4), 2001: 643-652. https://doi.org/10.1006/jsvi.2000.3311

[6] Y. Narita, Combinations for the free-vibration behaviors of anisotropic rectangular plates under general edge conditions. *Journal of Applied Mechanics*, 67(3), 2000: 568-573. https://doi.org/10.1115/1.1311959

[7] A. Bahrami, M.N. Bahrami, M.R. Ilkhani, Comments on "New exact solutions for free vibrations of thin orthotropic rectangular plates". *Composite Structures*, 107, 2014: 745-746. https://doi.org/10.1016/j.compstruct.2013.09.064

[8] M. Eisenberger, A. Deutsch Solution of thin rectangular plate vibrations for all combinations of boundary conditions. *Journal of Sound and Vibration*, 452, 2019: 1-12. https://doi.org/10.1016/j.jsv.2019.03.024

[9] G.R. Gavalas, M. El-Raheb, Extension of Rayleigh-Ritz method for eigenvalue problems with discontinuous boundary conditions applied to vibration of rectangular plates. *Journal of Sound and Vibration*, 333(17), 2014: 4007-4016. https://doi.org/10.1016/j.jsv.2014.03.030

[10] X. Liu, J.R. Banerjee, Free vibration analysis for plates with arbitrary boundary conditions using a novel spectral-dynamic stiffness method. *Computers and Structures*, 164, 2016: 108-126. https://doi.org/10.1016/j.compstruc.2015.11.005

[11] W. He, W. Chen, H. Qiao, In-plane vibration of rectangular plates with periodic inhomogeneity: Natural frequencies and their adjustment. *Composite Structures*, 105, 2013: 134-140.

https://doi.org/10.1016/j.compstruct.2013.05.013

[12] X. Shi, D. Shi, W.L. Li, Q. Wang, A unified method for free vibration analysis of circular, annular and sector plates with arbitrary boundary conditions. *Journal of Vibration and Control*, 22(2), 442-456. https://doi.org/10.1177/1077546314533580

[13] L. Najarzadeh, B. Movahedian, M. Azhari, Free vibration and buckling analysis of thin plates subjected to high gradients stresses using the combination of finite strip and boundary element methods. *Thin-Walled Structures*, 123, 2016: 36-47. https://doi.org/10.1016/j.tws.2017.11.015

[14] K. Mahapatra, S.K. Panigrahi, Dynamic response and vibration power flow analysis of rectangular isotropic plate using Fourier series approximation and mobility approach. *Journal of Vibration Engineering and Technologies*, 8, 2020: 105-119. https://doi.org/10.1007/s42417-018-0079-3

[15] H. Li, F. Pang, H. Chen, Y. Du, Vibration analysis of functionally graded porous cylindrical shell with arbitrary boundary restraints by using a semi-analytical method. *Composites Part B: Engineering*, 164, 2019: 249-264. https://doi.org/10.1016/j.compositesb.2018.11.046

[16] R. Li, X. Zheng, P. Wang, B. Wang, H. Wu, Y. Cao, Z. Zhu, New analytic free vibration solutions of orthotropic rectangular plates by a novel symplectic approach. *Acta Mechanica*, 230, 2019: 3087-3101. https://doi.org/10.1007/s00707-019-02448-1

[17] S. Zhang, L. Xu, R. Li, New exact series solutions for transverse vibration of rotationally-restrained orthotropic plates. *Applied Mathematical Modelling*, 65, 2019: 348-360. https://doi.org/10.1016/j.apm.2018.08.033

[18] M. Chen, G. Jin, T. Ye, Y. Zhang, An isogeometric finite element method for the in-plane vibration analysis of orthotropic quadrilateral plates with general boundary restraints. *International Journal of Mechanical Sciences*, 133, 2017: 846-862. https://doi.org/10.1016/j.ijmecsci.2017.09.052

[19] R. Li, P. Wang, Z. Yang, J. Yang, L. Tong, On new analytic free vibration solutions of rectangular thin cantilever plates in the symplectic space. *Applied Mathematical Modelling*, 53, 2018: 310-318. https://doi.org/10.1016/j.apm.2017.09.011

[20] R. Li, Y. Tian, P. Wang, Y. Shi, B. Wang, "New analytic free vibration solutions of rectangular thin plates resting on multiple point supports. *International Journal of Mechanical Sciences*, 110, 2016: 53-61. https://doi.org/10.1016/j.ijmecsci.2016.03.002

[21] R. Li, B. Wang, G. Li, B. Tian, Hamiltonian system-based analytic modeling of the free rectangular thin plates' free vibration. *Applied Mathematical Modelling*, 40(2), 2016: 984-992. https://doi.org/10.1016/j.apm.2015.06.019

[22] S. Ullah, Y. Zhong, J. Zhang, Analytical buckling solutions of rectangular thin plates by straightforward generalized integral transform method. *International Journal of Mechanical Sciences*, 152, 2019: 535-544. https://doi.org/10.1016/j.ijmecsci.2019.01.025

[23] S. Ullah, H. Wang, X. Zheng, J. Zhang, Y. Zhong, R. Li, New analytic buckling solutions of moderately thick clamped rectangular plates by a straightforward finite integral transform method. *Archive of Applied Mechanics*, 89, 2019: 1885-1897. https://doi.org/10.1007/s00419-019-01549-6